

Finite Element Analysis of Wing-Engine Assembly

KHIEM VIET NGO
Department of Aeronautics and Astronautics
Stanford University
Stanford, CA 94305-4035
UNITED STATES OF AMERICA
khiem.ngo@stanford.edu

Abstract: - When an aircraft is in operation, it is subject to many aerodynamic loads, among which lift and drag are the two most fundamental that have a direct impact on aircraft performance; particularly the wings. From structural engineering point of view, when one of these loads acts on the wing, it resembles a beam acted upon by a force distribution on top. Indeed, the objective of this research is to gain some fundamental understandings about the big picture of aircraft wing structures in the context of beam theory. Although wing structures have been studied by many researchers, research to date showed that the engines were not considered and analyzed together with the wing. Therefore, an integrated structural behavior of the wing and engines can never be fully understood. It is therefore the objective of this study is to show the structural impact of the engines on the wing, subject to an aerodynamic force, lift, and its variations in time.

Key-Words: - Eigenfrequency, eigenmode, spatial distribution, lift contribution, Rayleigh damping, orthogonal damping, dynamic response, deformation response factor

1 Introduction

Aircraft wing structures have been studied by many researchers but, up to date, it seems that none has actually showed the structural impact of the engines on the wings, especially when they are subject to an aerodynamic force, lift, which is formed by the free-stream density, free-stream velocity, and circulation. As such, some aspects of this investigation involve fluid-structure interactions between the air, a compressible fluid, and the wing itself. The wing and engine structures are usually considered separately in separate paths and, therefore, the resultant impact has never been fully understood. This paper will first consider the integrated structural behaviors of both the wing and the engines and then the wing individually so that the structural impact of the engines themselves on the wing will be revealed and better understood.

Another objective of this research is to gain some fundamental understandings about the big picture of aircraft wing structures in the context of beam theory. The wing can be thought of as a cantilever beam clamped on one end to the fuselage and freed on the other. As such, one can model the structural vibration of a wing as a clamped-free beam. To capture the structural dynamics of the wings and, particularly the engines, in details, the finite element lumped-mass approach will be employed. Likewise, to capture the structural dynamics of the wing itself, although it is best to use the lumped-mass approach again for the sake of comparisons, we are to use an energy method, namely the Rayleigh-Ritz, just for a

difference! Generally speaking, we are interested in knowing the vibration responses in terms of displacements, rotations, forces, and moments at the inner engine, mid-span, outer engine, and at the wing tip respectively. As such, the analysis employs a four-element model, which results in four modes of vibration. For a credible and realistic result, further considered are the effects of damping on each mode which make the responses decay in time. While damping can come in different forms, it can be assumed to be proportional to either the mass matrix, the stiffness matrix, or both, so that the entire coupled system can be uncoupled by using the undamped mode shapes. The analysis here considers the Rayleigh damping and general orthogonal damping and a comparison on the results is made between them. Finally, the dynamic deformation response is analyzed for each mode, subject to a sinusoidal time-variation function of lift.

In general, it is important to have a big picture, and as details as one can go, on the wing structural dynamics of a two-engine aircraft, such as the one considered herein. The wing is subject to many different aerodynamic loads when it is in the air, such as lift and drag, and different loads when it is on ground. These loads are generated by the density, pressure, velocity, circulation, . . . , of the air. Thus, it is important for one to understand the aerodynamic impact on aircraft structures, such as fluid-structure interactions, for the enhancement of aircraft performance and for the sake of safety. Today, aircraft developing companies, such as

Boeing, Lockheed, NASA, and others, have continually improved aircraft performance to achieve, among other goals, higher speeds. An open question for research could be: what happens to the structural performance of the wings, engines, or even the fuselage, when the aircraft flies at an incredible speed of Mach 7? Evidently, the dominant impact comes from aerodynamic loads, which could lead to structural failures of some devices. While it sounds more like a question for military fighters, it deserves a worthwhile recognition for research and this paper addresses an aspect of these.

2 Mathematical Model Formulation

What follows are the formulations of the wing structural model, the elliptical lift distribution, the Rayleigh-Ritz approach, and the effects of damping on the vibration of the wing. We begin our analysis with the following wing-engine assembly model:

2.1 Wing Structural Model Formulation

Using beam theory, the structure of an aircraft wing is modeled as a clamped-free cantilever beam. Assume that the wing has mass m , length L , Young modulus E , and moment of inertia I , the wing without engines takes a familiar shape, depicted in Figure 1 below.

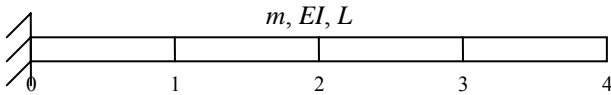


Figure 1 depict of an aircraft wing

When aircraft engines are considered together with the wing, the wing mass becomes relatively small compared to the mass of the engines. Therefore, the lumped-mass approach is best to use for both finite element and modal analyses. In using this approach we first lump the mass of the wing, without engines, into three masses, which are at a distance of $L/2$ apart. The lumped masses are $0.25m$, $0.5m$, and $0.25m$ respectively, Figure 2a. Now let us consider the mass of the engines. Suppose the wing carries two engines; one of mass $8m$ at a distance of $L/4$ from the fuselage, and the other $4m$ at a distance of $L/4$ from the wing tip, Figure 2b. Now add the two lumped-mass models together, an integrated lumped-mass model for both wing and engines results, Figure 2c.

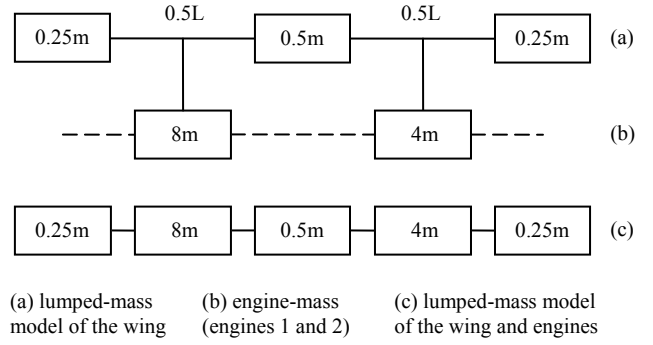


Figure 2 lumped-mass model of the wing and engines

The lumped-mass model divides the wing into four equal elements, each of length $L/4$. It suffices to use a four-element model. Note that the wing is clamped on the left end. As such, the left-most mass has neither vertical nor rotational displacement. Consequently, the mass matrix is reduced to a four-by-four matrix. Also, since each element has two degrees of freedom at each end (vertical and rotational), the stiffness matrix for each element is a four-by-four matrix as obtained below:

$$\mathbf{M} = \frac{mL}{8} \begin{bmatrix} 8 & & & \\ & .5 & & \\ & & 4 & \\ & & & .25 \end{bmatrix}$$

$$\mathbf{K}_i = \frac{64EI}{L^3} \begin{bmatrix} 12 & 1.5L & -12 & 1.5L \\ 1.5L & .25L^2 & -1.5L & .125L^2 \\ -12 & -1.5L & 12 & -1.5L \\ 1.5L & .125L^2 & -1.5L & .25L^2 \end{bmatrix}$$

Upon assembling the elemental stiffness matrices, the stiffness matrix for the wing is

$$\mathbf{K} = \frac{64EI}{L^3} \begin{bmatrix} \mathbf{K}_{vv} & \mathbf{K}_{vr} \\ \mathbf{K}_{rv} & \mathbf{K}_{rr} \end{bmatrix} \quad (1)$$

where

$$\mathbf{K}_{vv} = \begin{bmatrix} 24 & -12 & & \\ -12 & 24 & -12 & \\ & -12 & 24 & -12 \\ & & -12 & 12 \end{bmatrix} \quad \mathbf{K}_{vr} = L \begin{bmatrix} 0 & 1.5 & & \\ -1.5 & 0 & 1.5 & \\ & -1.5 & 0 & 1.5 \\ & & -1.5 & -1.5 \end{bmatrix}$$

$$\mathbf{K}_{rv} = L \begin{bmatrix} 0 & -1.5 & & \\ 1.5 & 0 & -1.5 & \\ & 1.5 & 0 & -1.5 \\ & & 1.5 & -1.5 \end{bmatrix} \quad \mathbf{K}_{rr} = L^2 \begin{bmatrix} .5 & .125 & & \\ .125 & .5 & .125 & \\ & .125 & .5 & .125 \\ & & .125 & .25 \end{bmatrix}$$

Suppose for the moment that we are concerned ourselves with only the vertical DOFs at each mass. Thus, we can statically condense the rotational degrees of freedom so that the stiffness matrix, in the absence of rotational DOFs, is simply a four-by-four matrix below

$$\hat{\mathbf{K}} = \mathbf{K}_{vv} - \mathbf{K}_{vr} \mathbf{K}_{rr}^{-1} \mathbf{K}_{rv}$$

$$= \frac{EI}{L^3} \begin{bmatrix} 1203 & -756 & 285 & -48 \\ -756 & 918 & -614 & 166 \\ 285 & -614 & 633 & -234 \\ -48 & 166 & -234 & 103 \end{bmatrix}$$

It is clear that the equation of motion that governs the vibration of the wing is of the form

$$\mathbf{M}\{\ddot{\mathbf{u}}\} + \mathbf{C}\{\dot{\mathbf{u}}\} + \hat{\mathbf{K}}\{\mathbf{u}\} = \mathbf{L}(t) \quad (2)$$

where $\mathbf{L}(t)$ is the lift distribution on top of the wing. As usual, one first considers the free vibration of the undamped system to obtain the undamped mode shapes and their natural frequencies. Using separation of variables in space and time, we solve the associated eigenvalue problem $(\hat{\mathbf{K}} - \omega^2 \mathbf{M})\{\mathbf{q}\} = \{\mathbf{0}\}$. Omitting the lengthy algebras, the eigenfrequencies are found to be

$$\omega_1 = \frac{3.41}{L^2} \sqrt{\frac{EI}{m}}, \quad \omega_2 = \frac{20.55}{L^2} \sqrt{\frac{EI}{m}},$$

$$\omega_3 = \frac{51.84}{L^2} \sqrt{\frac{EI}{m}}, \quad \omega_4 = \frac{131.67}{L^2} \sqrt{\frac{EI}{m}}$$

and the corresponding eigenmodes of vibration are

$$\{\mathbf{q}\}_1 = \begin{Bmatrix} 0.1007 \\ 0.3467 \\ 0.6654 \\ 1 \end{Bmatrix}, \quad \{\mathbf{q}\}_2 = \begin{Bmatrix} -0.5070 \\ -0.5506 \\ 0.0953 \\ 1 \end{Bmatrix},$$

$$\{\mathbf{q}\}_3 = \begin{Bmatrix} 0.0682 \\ -0.2340 \\ -0.0993 \\ 1 \end{Bmatrix}, \quad \{\mathbf{q}\}_4 = \begin{Bmatrix} -0.1150 \\ 2.3122 \\ -0.2097 \\ 1 \end{Bmatrix}$$

Figure 3 shows the eigenmodes of the wing, which are also called the undamped mode shapes, or simply modes, in physical terms. What is important is that all possible shapes of the wing resulted from any vibration can be mathematically expressed as a linear superposition of these four modes. Note that the bar plots reflect the true mode shapes whereas the curves that connect these bars represent typical

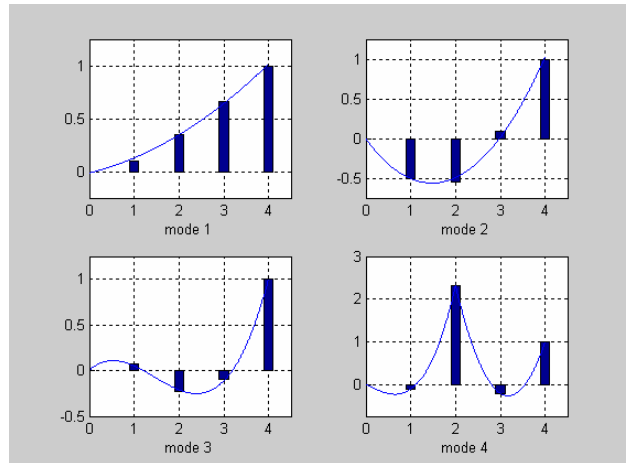


Figure 3 natural modes of vibration

continuous functions that fit the discrete shape of each mode. As such, the curves are not 100% accurate, especially at the left end where the displacement and rotation (slope) must be zero since the wing is clamped there. The number of mode shapes corresponds to the number of elements used in a finite element model. In practice, one must use as many elements as possible to achieve an accurate result. When more elements are used, more mode shapes are generated. However, only the first few that correspond to the low natural frequencies actually have a major impact and/or contribution to the overall vibration of the wing. Some analysis shows that high order modes, those associated with high frequencies, are usually inaccurate and that their contributions are just a matter of a few percent. Another importance of these undamped mode shapes is that, when they are used together in the form of a matrix, eigenvector matrix, they can help uncouple a system of differential equations due to their beautiful orthogonality properties! To this end, in order to make the mode shapes useful for subsequent computations, we normalize them with respect to the mass matrix \mathbf{M} . In doing so, we assume the normalized modes take the form $\{\boldsymbol{\phi}\}_i = c_i \{\mathbf{q}\}_i$, then solving the equation $\{\boldsymbol{\phi}\}_i^T [\mathbf{m}] \{\boldsymbol{\phi}\}_i = 1$ for the coefficients c_i 's, the normalized eigenmodes are

$$\{\boldsymbol{\phi}\}_1 = \frac{1}{\sqrt{mL}} \begin{Bmatrix} 0.1937 \\ 0.6674 \\ 1.2798 \\ 1.9234 \end{Bmatrix}, \quad \{\boldsymbol{\phi}\}_2 = \frac{1}{\sqrt{mL}} \begin{Bmatrix} -0.9080 \\ -0.9861 \\ 0.1707 \\ 1.7909 \end{Bmatrix}$$

$$\{\boldsymbol{\phi}\}_3 = \frac{1}{\sqrt{mL}} \begin{Bmatrix} 0.3240 \\ -1.1118 \\ -0.4718 \\ 4.7511 \end{Bmatrix}, \quad \{\boldsymbol{\phi}\}_4 = \frac{1}{\sqrt{mL}} \begin{Bmatrix} -0.1817 \\ 3.6533 \\ -0.3313 \\ 1.5800 \end{Bmatrix}$$

Now suppose the lift force vector $\mathbf{L}(t)$ can be expressed as the product of the time variation function $g(t)$, and their spatial distribution \mathbf{s} , $\mathbf{L}(t) = \{\mathbf{s}\}g(t)$, the contribution of the n th mode to the excitation vector \mathbf{s} is: $\{\mathbf{s}\}_n = \Gamma_n[\mathbf{m}]\{\boldsymbol{\phi}\}_n = \{\boldsymbol{\phi}\}_n^T \{\mathbf{s}\}[\mathbf{m}]\{\boldsymbol{\phi}\}_n$.

2.2 Elliptical Lift Distribution

In reality, lift distribution is of an elliptic shape. We know from aerodynamic theory that lift is generated from circulation, which varies elliptically with distance x along the span, i.e., if Γ_0 is the circulation at the clamped area, then the circulation Γ at any point x along the wing is $\Gamma(x) = \Gamma_0\sqrt{1-(x/L)^2}$. By Kutta-Joukowski theorem, lift distribution is equal to $L(x) = \rho_\infty V_\infty \Gamma(x)$, where ρ_∞ and V_∞ are the free-stream density and free-stream velocity respectively. Hence, it is clear that lift has an elliptical distribution due to an elliptical circulation. This kind of distribution perfectly makes sense since higher lifts are needed in the areas closer to the inner engine and, more specifically, to the fuselage, so that they can efficiently bring the aircraft body up. Also in this sense, the lifts should be lowest at the wing tip to avoid any crack that may occur due to large bending moment there.

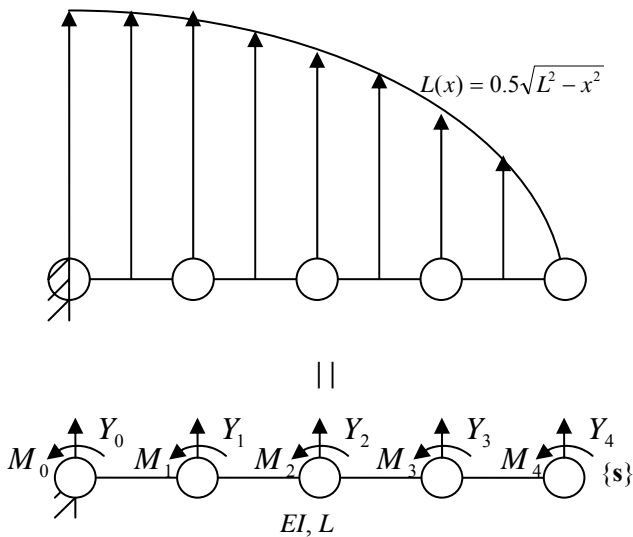


Figure 4 (a) elliptical lift distribution
(b) equiv. spatial distribution $\{\mathbf{s}\}$

As the preference herein is on the large picture of wing structural dynamics, we choose not to go to these details. Rather, we assume an elliptical lift distribution of the form $L(x) = 0.5\sqrt{L^2 - x^2}$. In order to use this load in the finite element context, we discretize it to obtain an equivalent spatial distribution $\mathbf{s} = [Y_0, Y_1, Y_2, Y_3, Y_4]$ at the masses, using the finite element mode shapes below:

$$f_1(x) = 1 - 3\frac{x^2}{(L/4)^2} + 2\frac{x^3}{(L/4)^3}$$

$$f_2(x) = x - 2\frac{x^2}{(L/4)} + \frac{x^3}{(L/4)^2}$$

$$f_3(x) = 3\frac{x^2}{(L/4)^2} - 2\frac{x^3}{(L/4)^3}$$

$$f_4(x) = -\frac{x^2}{L/4} + \frac{x^3}{(L/4)^2}$$

In other words, if R is the reaction at the left end,

$$Y_0 = \int_0^{L/4} L(x)f_1(x)dx + R$$

$$Y_1 = \int_0^{L/4} L(x)f_3(x)dx + \int_{L/4}^{L/2} L(x)f_1(x)dx$$

$$Y_2 = \int_{L/4}^{L/2} L(x)f_3(x)dx + \int_{L/2}^{3L/4} L(x)f_1(x)dx$$

$$Y_3 = \int_{L/2}^{3L/4} L(x)f_3(x)dx + \int_{3L/4}^L L(x)f_1(x)dx$$

$$Y_4 = \int_{3L/4}^L L(x)f_3(x)dx$$

Note that in order for the wing to be in equilibrium, the sum of all the Y_i 's must be equal to zero. As said, the interest here is to know the displacement and rotation at the masses. Since the wing is clamped on the left end, Y_0 cannot give rise to any displacement and rotation there ($v_0 = \theta_0 = 0$). It follows that the spatial distribution is reduced to a four by one column vector: $\mathbf{s} = [Y_1, Y_2, Y_3, Y_4]^T = [0.229, 1.304, 1.368, -2.571]^T$. In the same fashion, the moment equations can be expressed using the above shape functions:

$$\begin{aligned}
M_0 &= \int_0^{L/4} L(x)f_2(x)dx + M_R \\
M_1 &= \int_0^{L/4} L(x)f_4(x)dx + \int_{L/4}^{L/2} L(x)f_2(x)dx \\
M_2 &= \int_{L/4}^{L/2} L(x)f_4(x)dx + \int_{L/2}^{3L/4} L(x)f_2(x)dx \\
M_3 &= \int_{L/2}^{3L/4} L(x)f_4(x)dx + \int_{3L/4}^L L(x)f_2(x)dx \\
M_4 &= \int_{3L/4}^L L(x)f_4(x)dx
\end{aligned}$$

Let us now consider the rotational DOFs together with the displacement DOFs, it can be seen from (1) that the displacement, rotation, shear force, and moment at each mass are all related in the following equation

$$\begin{Bmatrix} \mathbf{Y} \\ \mathbf{M} \end{Bmatrix} = \begin{bmatrix} \mathbf{K}_{vv} & \mathbf{K}_{vr} \\ \mathbf{K}_{rv} & \mathbf{K}_{rr} \end{bmatrix} \begin{Bmatrix} \mathbf{v} \\ \boldsymbol{\theta} \end{Bmatrix}$$

where $\mathbf{Y} = [Y_1, Y_2, Y_3, Y_4]^T$, $\mathbf{M} = [M_1, M_2, M_3, M_4]^T$, $\mathbf{v} = [v_1, v_2, v_3, v_4]^T$, and $\boldsymbol{\theta} = [\theta_1, \theta_2, \theta_3, \theta_4]^T$. It follows that the nodal displacement and rotation, at the masses, for $L = 1$, are

$$\begin{Bmatrix} v_1 \\ v_2 \\ v_3 \\ v_4 \\ \theta_1 \\ \theta_2 \\ \theta_3 \\ \theta_4 \end{Bmatrix} = \frac{1}{EI} \begin{Bmatrix} 0.0080 \\ 0.0288 \\ 0.0574 \\ 0.0909 \\ 0.0606 \\ 0.1044 \\ 0.1370 \\ 0.1577 \end{Bmatrix}$$

Also, we have $v_0 = \theta_0 = 0$. Consequently the modal lift contributions with respect to \mathbf{s} are found to be

$$\begin{aligned}
\mathbf{s}_1 &= \begin{Bmatrix} -0.4414 \\ -0.0951 \\ -1.4584 \\ -0.1370 \end{Bmatrix}, & \mathbf{s}_2 &= \begin{Bmatrix} 5.3245 \\ 0.3614 \\ -0.5004 \\ -0.3282 \end{Bmatrix}, \\
\mathbf{s}_3 &= \begin{Bmatrix} -4.6122 \\ 0.9891 \\ 3.3577 \\ -2.1134 \end{Bmatrix}, & \mathbf{s}_4 &= \begin{Bmatrix} -0.0374 \\ 0.0470 \\ -0.0341 \\ 0.0102 \end{Bmatrix}
\end{aligned}$$

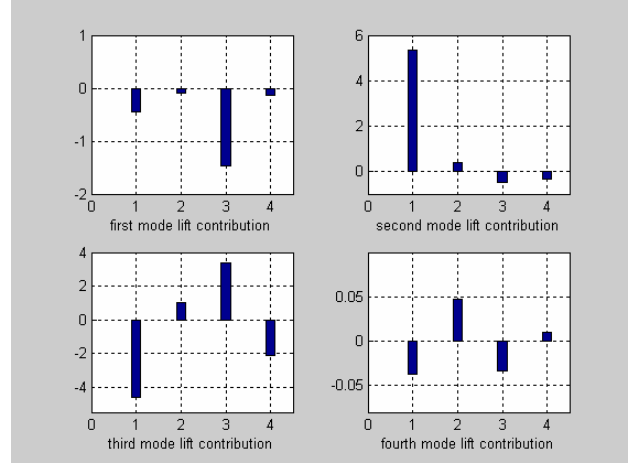


Figure 5 modal lift contribution w.r.t. lift distribution

It is clear from Figure 5 that the lift contributions in these modes are mostly dominated by the first and the third mass, where the two engines are located. In addition, the engines give rise to large variations in lift as compared to those at the other masses. To be more specific, the first mode contributes negative lift distribution at every mass. Contribution from the second mode is totally dominated by the lift contributed by the inner engine. As for the third mode, negative lifts are generated at the inner engine and at the wing tip while some positive lifts are generated at the masses in between. The fourth mode has little lift contribution and so it could be ignored from further consideration. Nevertheless, for a complete analysis, this mode will be retained in the subsequent calculations. Thus, Figure 5 indicates that the heavier the mass is, the more variations in lift it causes and that these variations may include negative lifts. In the section to come, we are to examine the structural impact of the engines on the wing in terms of the displacements and rotations at the masses.

So far, we have discussed about the modal lift contributions and vibration of the wing when the mass of the two engines are attached to the wing. To explore the impact of the two engines on the wing, it is important to consider the wing individually so that one can see the difference and that a conclusion can be drawn from. Hence, we are back with the simple equation of motion that governs the motion of a beam. Many methods can be employed; lumped-mass, consistent-mass, modal analysis, Rayleigh-Ritz method, ... Though it is best to use the lumped-mass approach again for the sake of comparison, let us go with the Rayleigh-Ritz method, which will be used along with the principle of minimum potential energy. In using this method, the mass of the wing

is not lumped and so one can expect a slight difference in the result!

2.3 Rayleigh-Ritz Method

For the Rayleigh-Ritz, we first assume a trial function that describes the wing motion. To satisfy the geometric boundary condition, we let the displacement $\omega(x) = c_1x^2 + c_2x^3$. Then, the strain energy for the wing can be expressed in terms of the strain energy for the beam, i.e.

$$\begin{aligned} U &= \int_0^L \frac{M^2(x)}{2EI} dx = \int_0^L \frac{[EI\omega''(x)]^2}{2EI} dx \\ &= \frac{EI}{2} \int_0^L (2c_1 + 6c_2x)^2 dx \\ &= EI(2c_1^2L + 6c_1c_2L^2 + 6c_2^2L^3) \end{aligned}$$

Similarly, the potential energy due to the external force, lift $L(x)$, is

$$\begin{aligned} V &= - \int_0^L L(x)\omega(x) dx \\ &= - \frac{1}{2} \int_0^L (c_1x^2 + c_2x^3) \sqrt{L^2 - x^2} dx \\ &= - \frac{\pi L^4}{32} c_1 - \frac{L^5}{15} c_2 \end{aligned}$$

Thus, the total energy is

$$\begin{aligned} \Pi &= U + V \\ &= EI \begin{bmatrix} c_1 \\ c_2 \end{bmatrix}^T \begin{bmatrix} 2L & 3L^2 \\ 3L^2 & 6L^3 \end{bmatrix} \begin{bmatrix} c_1 \\ c_2 \end{bmatrix} - \begin{bmatrix} \pi L^4/32 \\ L^5/15 \end{bmatrix} \begin{bmatrix} c_1 \\ c_2 \end{bmatrix} \end{aligned}$$

By applying the principle of minimum potential energy, the maximum total energy is obtained at the point at which the energy rate of change is zero. In this sense, we mean

$$\frac{\partial \Pi}{\partial [c_1, c_2]^T} = EI \begin{bmatrix} 4L & 6L^2 \\ 6L^2 & 12L^3 \end{bmatrix} \begin{bmatrix} c_1 \\ c_2 \end{bmatrix} - \begin{bmatrix} \pi L^4/32 \\ L^5/15 \end{bmatrix} = \begin{bmatrix} 0 \\ 0 \end{bmatrix}$$

Solving these two equations, we obtain $c_1 = 0.0648L^3/EI$ and $c_2 = 0.0269L^2/EI$. Thus, the displacement of the wing is governed by

$$\omega(x) = \frac{L^5}{EI} \left(0.0648 \frac{x^2}{L^2} + 0.0269 \frac{x^3}{L^3} \right)$$

2.4 Effects of Damping

Up to now, all of the results have been obtained without the consideration of damping effects. This is quite ideal since we know that damping exists in every structure. Otherwise, a steady-state response could never be reached. Thus, for a reasonable solution, damping effects must be taken into account so that we can have a decaying solution as time gets large. While damping can come in different forms, let us consider two types of damping: Rayleigh damping and general orthogonal damping. Rayleigh damping is one in which the damping matrix is proportional to both the mass and stiffness matrix, that is, $\mathbf{C} = \alpha_0\mathbf{M} + \alpha_1\mathbf{K}$ for some coefficients α_0 and α_1 . From the analysis of Rayleigh damping (Appendix), α_0 and α_1 satisfy the equation

$$\frac{1}{2} \begin{bmatrix} 1/\omega_i & \omega_i \\ 1/\omega_j & \omega_j \end{bmatrix} \begin{Bmatrix} \alpha_0 \\ \alpha_1 \end{Bmatrix} = \begin{Bmatrix} \xi_i \\ \xi_j \end{Bmatrix}$$

Then

$$\begin{Bmatrix} \alpha_0 \\ \alpha_1 \end{Bmatrix} = \frac{2\omega_i\omega_j}{\omega_j^2 - \omega_i^2} \begin{bmatrix} \xi_i\omega_j - \xi_j\omega_i \\ -\xi_i/\omega_j + \xi_j/\omega_i \end{bmatrix}$$

Assuming that the damping ratios that corresponds to the first two modes are equal, $\xi_i = \xi_j$, then $\alpha_0 = 5.85\xi_i\sqrt{EI/m}$ and $\alpha_1 = 0.0833\xi_i\sqrt{m/EI}$. Recall from (2) that the equation of motion of the wing is

$$\mathbf{M}\{\ddot{\mathbf{u}}\} + \mathbf{C}\{\dot{\mathbf{u}}\} + \hat{\mathbf{K}}\{\mathbf{u}\} = \{\mathbf{s}\}g(t)$$

and that $\{\mathbf{u}\} = \mathbf{\Phi}\{\mathbf{y}\}$. By premultiplying the EOM equation by $\mathbf{\Phi}^T$ and postmultiplying it by $\mathbf{\Phi}$ and utilizing the orthogonality relations of eigenmodes, we have

$$\{\ddot{\mathbf{y}}\} + (\alpha_0 + \omega_i^2\alpha_1)\{\dot{\mathbf{y}}\} + \omega_i^2\{\mathbf{y}\} = \mathbf{\Phi}_i^T\{\mathbf{s}\}g(t)$$

Let $P_i(t) = \mathbf{\Phi}_i^T\{\mathbf{s}\}$ is the participation factor and $y_i(t) = P_i(t)D_i(t)$, we have

$$\ddot{D}_i + (\alpha_0 + \omega_i^2\alpha_1)\dot{D}_i + \omega_i^2D_i = g(t)$$

for $i = 1, \dots, 4$. To show damping effects, suppose the time variation function of lift is $g(t) = p_o \sin \omega t$ for $0 < t \leq \pi/2$ and, say, for the time being, we are only interested in the steady-state modal dynamic response. After some algebra, we have

$$D_i^{st}(t) = D_i^p(t) = A \sin \omega t + B \cos \omega t$$

where

$$A = \frac{1 - (\omega/\omega_i)^2}{\omega_i^2 [1 - (\omega/\omega_i)^2]^2 + \alpha_i^2(\xi)(\omega/\omega_i)^2} \quad (3)$$

$$B = \frac{-\alpha_i(\xi)(\omega/\omega_i)^2}{\omega_i^2 [1 - (\omega/\omega_i)^2]^2 + \alpha_i^2(\xi)(\omega/\omega_i)^2} \quad (4)$$

where $\alpha_i(\xi) = \alpha_0(\xi) + \omega_i^2 \alpha_1(\xi)$. Thus, the steady-state dynamic deformation factor of the system for $g(t) = p_o \sin \omega t$ can be written as

$$D_i^{st}(t) = (p_o/\omega_i^2) R_d \sin(\omega t - \phi)$$

where $R_d = D_o/D_o^{st} = \sqrt{A^2 + B^2}/(1/\omega_i^2)$ and $\phi = \tan^{-1}(-B/A)$. Likewise, one can obtain a similar result for the steady-state deformation factor $\tilde{R}_d = u_o/(u_{st})_o = \sqrt{\tilde{A}^2 + \tilde{B}^2}/(1/\omega_i^2)$ and its phase $\tilde{\phi} = \tan^{-1}(-\tilde{B}/\tilde{A})$.

As for the general orthogonal damping, the damping matrix \mathbf{C} is computed from the expression: $\mathbf{C} = \mathbf{M}\hat{\mathbf{C}}\mathbf{M}^T$, where $\hat{\mathbf{C}} = \text{diag}(2\xi_i\omega_i)$ is a diagonal matrix (Appendix). Thus for the general orthogonal damping, the coefficients A and B are

$$A = \frac{1}{\omega_i^2} \frac{1 - (\omega/\omega_i)^2}{[1 - (\omega/\omega_i)^2]^2 + [2\xi(\omega/\omega_i)]^2} \quad (5)$$

$$B = \frac{1}{\omega_i^2} \frac{-2\xi(\omega/\omega_i)}{[1 - (\omega/\omega_i)^2]^2 + [2\xi(\omega/\omega_i)]^2} \quad (6)$$

3 Results

3.1 Assumptions

In order to show the results graphically, let us compute the term $\sqrt{EI/m}$. Assuming the wing has a uniform rectangular cross section and that the wing length $L = 36$ feet, wing width $W = 4$ feet, and wing thickness $T = 0.5$ feet, so the wing volume is

72 cubic feet, or equivalently 124,416 cubic inches. Note that previous calculations assumed $L = 1$ and so, in order for everything to make sense, let us introduce a new unit, called “ngo” so that 1ngo = 36 feet. Thus the length L of the wing is equal to 1ngo, a reference value. As such, for computational purposes, we convert the units of E and I to lb/ngo^2 and ngo^4 respectively. The introduction of the unit “ngo” is only used for computational purposes and should not affect the outcome of the results!

A commonly used material for aircraft is Aluminum 7075-T6 [6-7], which has the Young modulus $E = 10.4 \times 10^6$ psi and density $\rho = 0.101$ lb/in³. Consequently, the weight of the wing is found to be 12,566 lbs. In addition, the moment of inertia equals $I = (1/12)T^3W = (1/12)(6'')^3(48'') = 864$ in⁴. It follows that $\sqrt{EI/m} = 846$ in = 1.96ngo.

In addition, we assume, at zero angle of attack, an elliptical lift distribution of the form $L(x) = 0.5\sqrt{L^2 - x^2}$ and a harmonic time variation function $g(t) = p_o \sin \omega t$. By discretizing $L(x)$ into concentrated loads at the masses, we obtain the followings

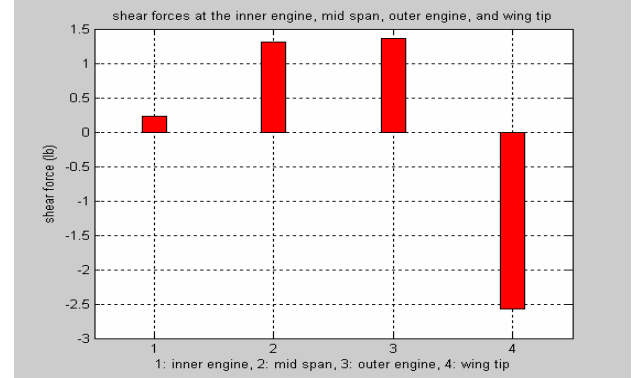


Figure 6 (a) spatial distribution of lift {s}

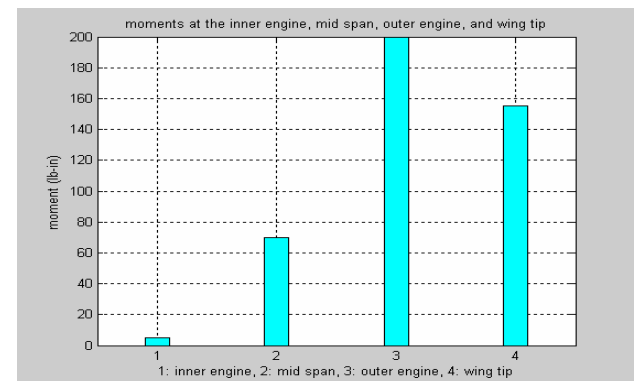


Figure 6 (b) the corresponding moments

3.2 Analysis of the Results

Below, we show the effect of the engine masses on the wing under aerodynamic loads, the effects of damping and the difference between Rayleigh and general orthogonal damping. In addition, we show the modal dynamic deformation response factors due to these two dampings.

3.2.1 Finite Element (with engines) vs. Rayleigh-Ritz (without engines)

The numerical results obtained for displacements and rotations at the inner engine, mid-span, outer engine, and at the wing tip are shown in Figure 7 and Figure 8. Note that, in these figures, we show the effects of the engine masses on the displacement and rotation of the wing, and not on the comparison between the lumped-mass and Rayleigh-Ritz approach. Recall that the mass of the two engines was included in the consideration of the lumped-mass approach; in the Rayleigh-Ritz, the engine mass was not included. It is in this purpose so that the structural impact of the engines can be revealed. Figure 7 shows displacements and Figure 8 rotations at the masses. The blue strips represent the finite element lumped-mass approach and the magenta represents the Rayleigh-Ritz. It is clear that the addition of the engine masses causes more displacements at the inner engines, mid-span, and outer engine while it is about the same at the wing tip. Consequently, these additional displacements give rise to additional rotations at the inner engine and the mid-span but they decrease as they reach the wing tip. Needless to say, the displacements get larger and larger close to the wing tip, so do the bending moments. Thus, the wing tip has the maximum displacement and, consequently, maximum bending moment. In general, the addition of the two engines slightly increases the displacements of the inner masses while it greatly decreases the large bending moment at the wing tip,

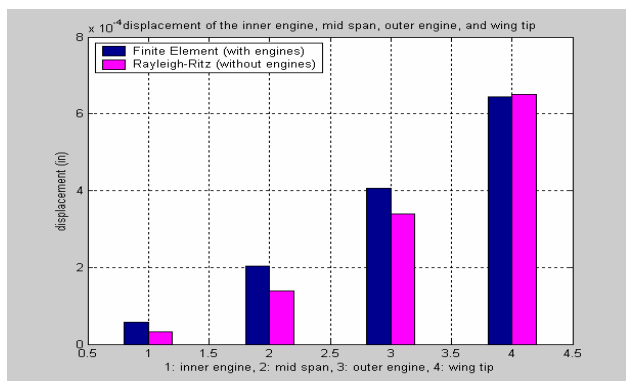


Figure 7 displacements of the masses

Figure 8. Interestingly enough, the displacement seems to vary linearly in the finite element lumped-mass approach while the same phenomenon happens for the rotation in the Rayleigh-Ritz.

3.2.2 Rayleigh vs. Orthogonal Damping

Figure 9 and Figure 10 show the vibration of each mode as a function of time and damping ratio for $\omega = 1$ and $p_o = 1$ under the effect of Rayleigh damping and general orthogonal damping. Note that the numbers on the x- and y-axes correspond to the for-loop iterations and hence do not mean anything. The modes are plotted for $0 \leq t \leq \pi/2$ and $0 \leq \xi \leq 1$ as indicated in each figure. As seen, the results are almost identical between the two dampings; they seem to have the same effects and on the vibration of the wing. As a matter of fact, the Rayleigh damping behaves more like a mass damping, a damping that is proportional to the mass matrix \mathbf{M} . It is because the stiffness damping coefficient α_1 is losing its effect, especially for small damping ratios ξ . In general, one can clearly see the effect of either damping on the modes; the amplitude of vibrations decays from the first mode with lowest frequency down to the fourth mode with highest frequency. In fact, the vibrations actually die out in the fourth mode. However, either damping seems to have a linear effect within each mode, with the exception of the first one. In fact, the results appear that either damping first has a nonlinear effect on lower mode (mode 1) and this effect becomes more linear in higher modes and eventually becomes constant. This is best seen in the general orthogonal damping. This shows that damping is losing its effect on higher modes although, globally speaking, it does force the amplitudes of higher modes to decay. Anyhow, as always, the lower modes are usually those of concern, not the higher modes, and this is something one can expect.

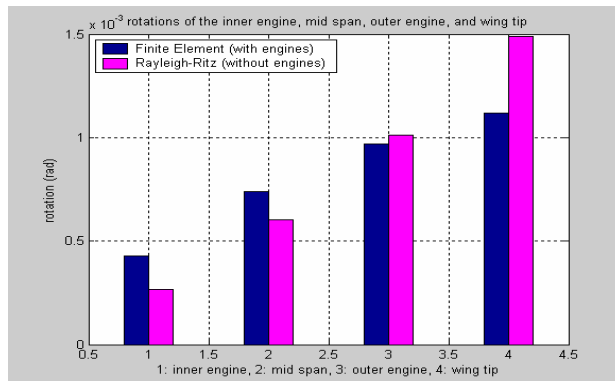
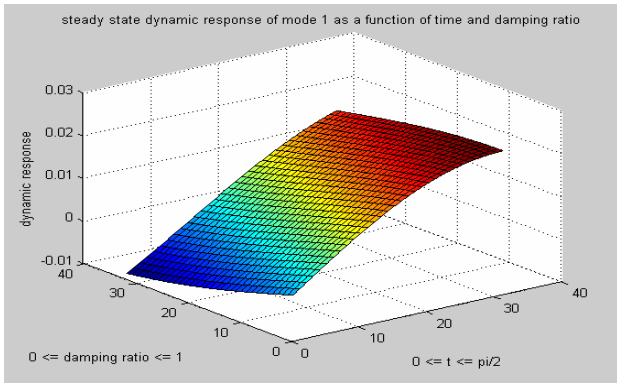


Figure 8 rotations at the masses

Rayleigh Damping



Orthogonal Damping

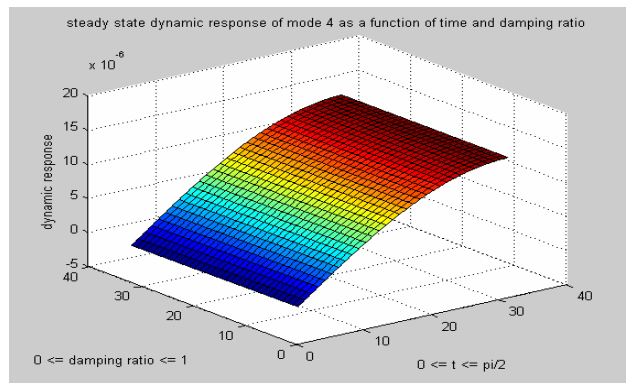
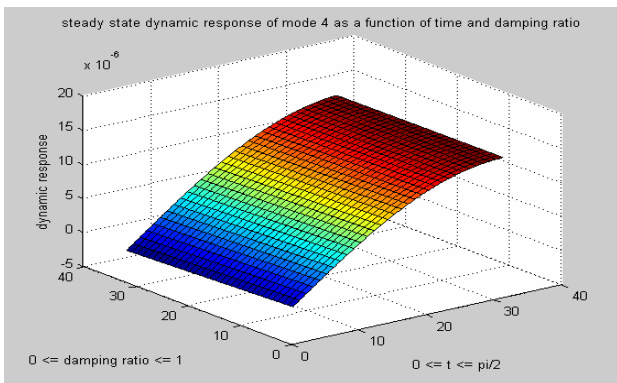
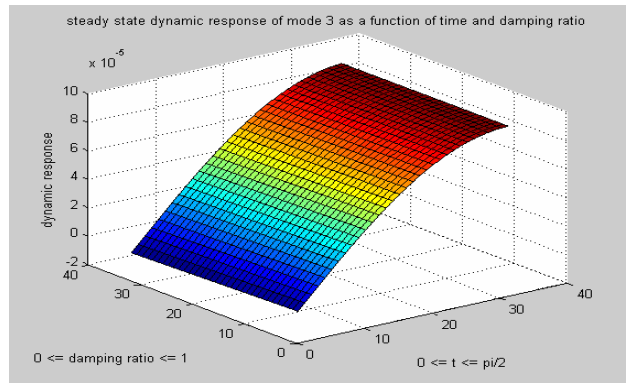
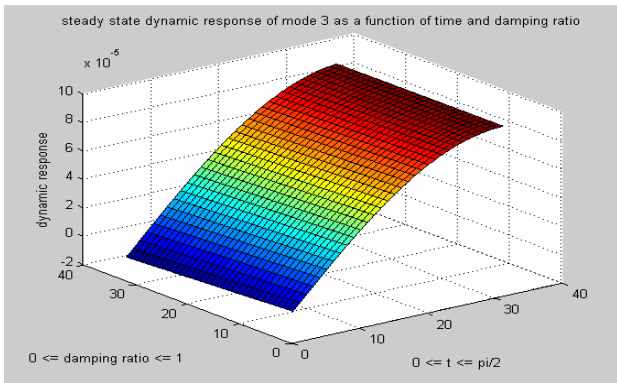
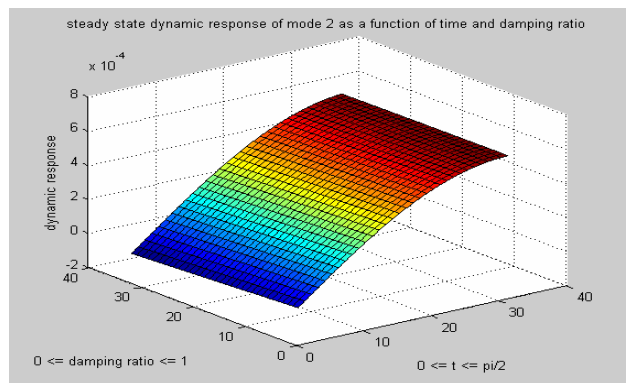
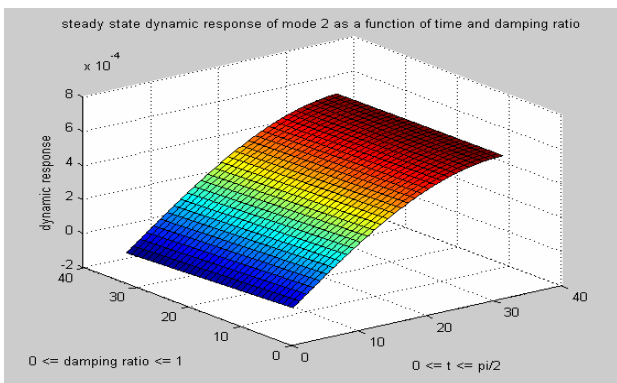
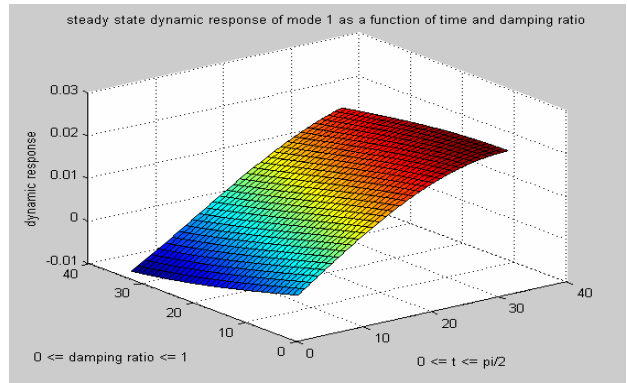


Figure 9(a,b,c,d)

Figure 10(a,b,c,d)

3.2.3 Modal Dynamic Deformation Response Factor Due To Rayleigh Damping

It follows from (3) and (4) that the modal dynamic deformation response factors and their corresponding phase angles are

$$R_{d_i} = \frac{1}{\sqrt{[1 - (\omega/\omega_i)^2]^2 + (\alpha_i/\omega_i)^2 (\omega/\omega_i)^2}} \quad (7)$$

$$\phi_i = \tan^{-1} \frac{\alpha_i (\omega/\omega_i)}{\omega_i [1 - (\omega/\omega_i)^2]} \quad (8)$$

which are shown in Figure 11. The values of R_d and ϕ are plotted for five different values of ξ . (Note that the values of $\xi = 0.01$ and $\xi = 0.03$ are plotted twice!) As can be expected, a resonance phenomenon occurs when the natural frequency is close to the frequency of the harmonic loading, especially at small damping ratios. For example, when $\xi = 0.01$, the amplitude of R_d reaches fifty at $\omega/\omega_i = 1$. This occurs at $\phi = 90^\circ$. So, the smaller the damping ratio, the higher amplitude the resonance reaches in the vicinity of $\omega/\omega_i = 1$ and this couples with a sharp change in the phase. If the natural frequency ω_n is away from the harmonic loading frequency ω , there is no concern! Recall that we assumed during the first $\pi/2 = 1.57$ seconds of flight, the variation of lift took the form of a harmonic sine wave with frequency ω . Thus the resonance can be avoided if ω of the harmonic lift variation is chosen to be away from ω_i of the free vibration of the undamped system. In general, stability can be restored in higher damping, which are shown in higher values of ξ .

In addition, the resonance amplitude decreases in higher modes. In Figure 11(a,b), the first two modes seems to have the same resonance amplitude but the last two, Figure 11(c,d), they decrease tremendously and this couples with a slow change in the phase angle. Thus again, the resonance is lessened in higher modes. In general, we can briefly summarize in a few observations as follows:

1. If the frequency ratio $\omega/\omega_i \ll 1$, that is, when the applied force is slowly varying R_d is just slightly larger than 1 and, therefore, is independent of damping. Thus, $D_o \cong D_o^{st} = p_o/\omega_i^2$. This result implies that the dynamic response is essentially the same as the static deformation and is controlled by the natural frequency, or more specifically, by the

stiffness of the system. It is because the stiffness becomes dominant when ω_i is small.

2. If $\omega/\omega_i \gg 1$, that is, when the applied force is rapidly varying, equation (7) shows that $R_d \rightarrow 0$ and is essentially unaffected by damping. At large ω/ω_i , it is seen again from (7) that $D_o \cong D_o^{st} \omega_i^2/\omega^2 = p_o/\omega^2$. This results implies that the response is controlled by the mass of the system, which consists of the masses of the inner and outer engines and the other lumped masses at the mid-span and wing tip.

3. If $\omega/\omega_i \cong 1$, that is, when the forcing frequency is close to the natural frequency of the system, R_d is very sensitive to damping as discussed above. This means that the dynamic deformation response can be much larger than the static (dynamic) deformation. More specifically, $\omega \cong \omega_i$ implies $D_o \cong D_o^{st}/\alpha_i \omega_i$ while $\alpha_i(\xi) = \alpha_0(\xi) + \omega_i^2 \alpha_1(\xi)$ is a function of damping ratio. Thus, this result shows that the response is controlled by the damping of the system.

Furthermore, the phase angle, which tells us about the time by which the response lags behind the force, can be examined based on the same three regions of the excitation-frequency scales:

1. If $\omega/\omega_i \ll 1$, (when the force is slowly varying), ϕ is close to 0° and the displacement is in phase with the applied force. That is, the system displaces itself to the same direction of the applied harmonic force. In addition, at the same damping ratio, the phase changes slowly at lower modes and more dramatically at higher modes.

2. If $\omega/\omega_i \gg 1$, (when the force is rapidly varying), ϕ is close to 180° and the displacement is out of phase with the applied force. In other words, the system displaces itself in a direction opposed to that of the applied harmonic force. Also, at the same damping ratio, the situation is reversed in that the phase changes rapidly at lower modes and more slowly in higher modes.

3. If $\omega/\omega_i \cong 1$, (when the forcing frequency is closed to the natural frequency), ϕ is close to 90° for all values of damping ratios ξ , and the displacement attains its peaks whenever the force passes through zeros.

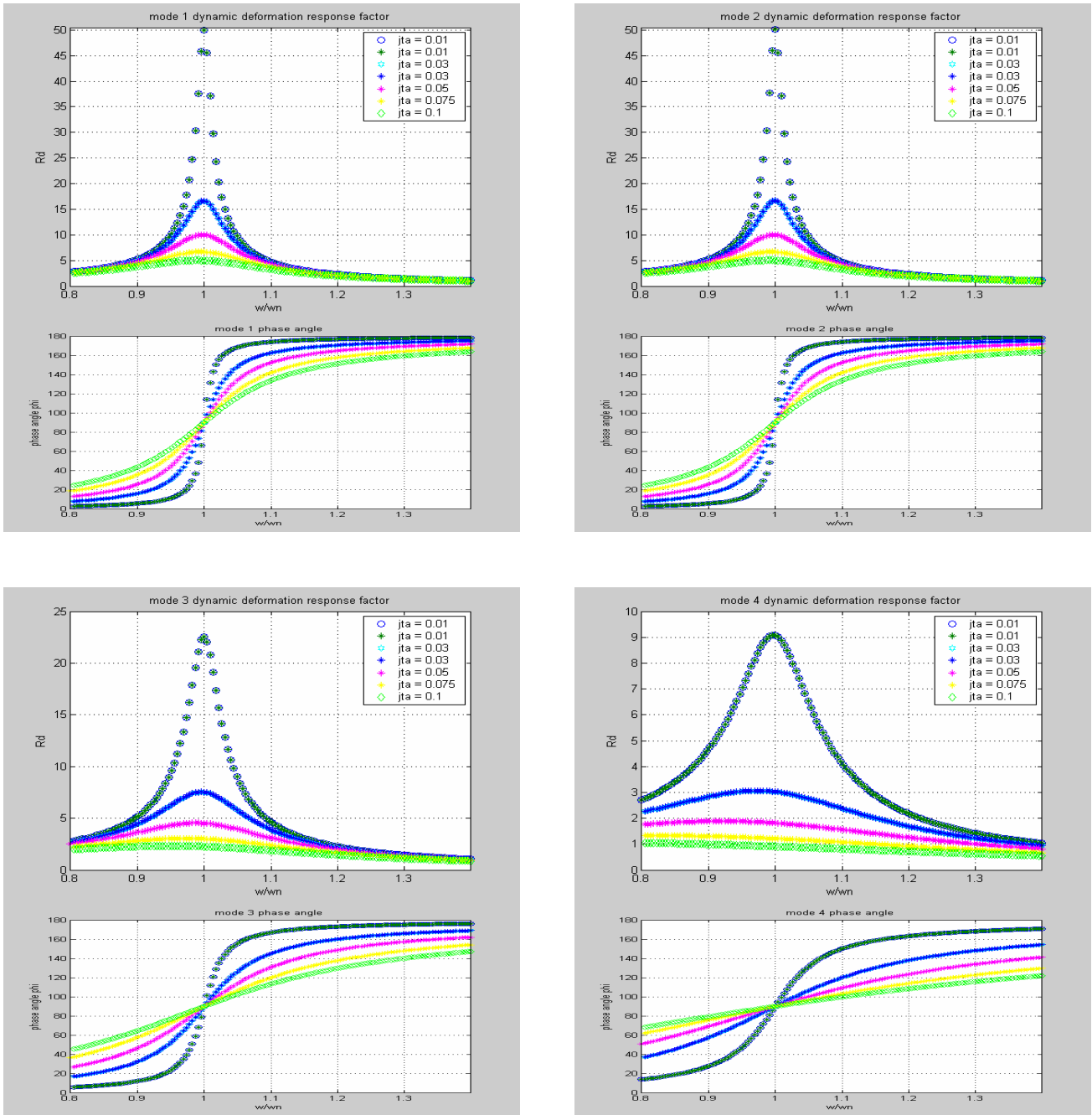


Figure 11 (a,b,c,d) modal dynamic deformation factor and phase angle under Rayleigh damping

3.2.4 Modal Dynamic Deformation Response Factor Due to Orthogonal Damping

Note that, for the general orthogonal damping, the dynamic deformation response factors are all the same for all four modes. Therefore, it suffices to plot one of them. It is easily seen if R_d and ϕ are plotted as a function of the frequency ratio ω/ω_n , in contrast with Rayleigh damping, the resonance is not lessened in higher modes in the general orthogonal damping because R_d and ϕ are the

same for all four modes. Also in this sense, the phase angles in higher modes are unaffected by damp-ing. Hence, for general orthogonal damping, although there are four modes, their behaviors are all the same as far as the effect of damping is concerned. Therefore, it would be redundant to consider higher modes in the general orthogonal damping! In general, the dynamic deformation response factor and its associate phase angle are the same as those of the first mode under in the Rayleigh damping.

4 Summary

In short, this study conducted some fundamental investigations of the wing structural dynamics in the context of beam theory, particularly, when the wing is under the effect of an aerodynamic load on top (lift) and its variation in time. The study analyzes the effect of engine masses on the displacements and rotations of the wing at nodal places, where the wing mass is lumped, by showing the difference in the results obtained by the finite element and Rayleigh-Ritz approach. Three main findings are highlighted:

Firstly, the analysis shows that the engine masses give rise to a little more displacements and rotations but they dramatically reduce the rotation at the wing tip. This is important because the wing tip has the largest bending moment and therefore needs to be reduced for stabilization and for avoidance of any potential crack that may occur.

Secondly, we consider the effect of damping within each mode, mode-wise, and between Rayleigh damping and general orthogonal damping. These two damping have almost identical modal effects; the steady state dynamic response is first nonlinear in the first mode and becomes more and more linear in higher modes and eventually constant at any given time. As such, higher modes are unaffected by damping. Note that steady state dynamic response is still nonlinear overall because of the harmonic applied force but, with respect to damping at any given time, it becomes more linear and eventually constant in higher modes. What's more, we analyze the modal dynamic deformation response factors and their associate phases in details. So again, some attentions must be paid when the time variation function is harmonic; which is usually the case during take-off and landing, particularly when its frequency is close to the natural frequency of the system; resonance occurs at all values of damping ratios, and is more severe when these values are small. As far as the effect of damping is concerned, higher damping helps damps out the resonance amplitudes and their associated phases.

Thirdly, when the applied force is harmonic, some important observations about its effect are as follows: At low frequency ratio, it is shown that the response is controlled by the stiffness of the system whereas at high frequency ratio the response is controlled by the mass of the system, and lastly, when the forcing frequency is close to the natural frequency, the response is controlled by the damping of the system. In the same fashion, the response is in phase at low frequency ratio, out of phase at high frequency ratio, and is peak when the forcing function passes its zeroes.

References:

- [1] Z. Kusculuoglu, B. Fallahi, and T. Royston, Finite Element Model of a Beam with a Piezo-ceramic Patch Actuator, *Journal of Sound and Vibration*, Vol.276, pp.27-44, 2004
- [2] B. Yardimoglu and T. Yildirim, Finite Element Model for Vibration Analysis of Pre-twisted Timoshenko Beam, *Journal of Sound and Vibration*, Vol.273, pp.741-754, 2004
- [3] T. Yang, *Finite Element Structural Analysis*, ISBN: 0-13-317116-7 Prentice Hall
- [4] A. Chopra, *Dynamics of Structures: Theory and Applications to Earthquake Engineering*, ISBN: 0-13-855214-2, Prentice Hall
- [5] J. Anderson Jr, *Fund. of Aerodynamics*, ISBN: 0-07-237335-0, McGraw Hill
- [6] C. Sun, *Mechanics of Aircraft Structures*, ISBN: 0-471-17877-2, Wiley & Sons
- [7] Beer and Johnston, *Mechanics of Materials*, ISBN: 0-07-911388-5, McGraw Hill

Appendix:

▪ Rayleigh Damping

If we premultiply the damping matrix by $\{\mathbf{q}\}_i^T$ and postmultiply by $\{\mathbf{q}\}_i$, we have

$$c_{ij}^* = \{\mathbf{q}\}_i^T [\mathbf{C}] \{\mathbf{q}\}_i = \begin{cases} c_{ii}^*, & i = j \\ 0, & i \neq j \end{cases}, \text{ where}$$

$$\begin{aligned} c_{ii}^* &= \alpha_0 \{\mathbf{q}\}_i^T [\mathbf{M}] \{\mathbf{q}\}_i + \alpha_1 \{\mathbf{q}\}_i^T [\mathbf{K}] \{\mathbf{q}\}_i \\ &= \alpha_0 m_{ii}^* + \alpha_1 k_{ii}^* = 2\xi_i \omega_i m_{ii}^* \end{aligned}$$

It follows that $\xi_i = \frac{1}{2\omega_i} \alpha_0 + \frac{1}{2} \omega_i \alpha_1$ where α_0

and α_1 can be found by

$$\frac{1}{2} \begin{bmatrix} 1/\omega_i & \omega_i \\ 1/\omega_j & \omega_j \end{bmatrix} \begin{Bmatrix} \alpha_0 \\ \alpha_1 \end{Bmatrix} = \begin{Bmatrix} \xi_i \\ \xi_j \end{Bmatrix}$$

▪ General Orthogonal Damping

The transformed damping matrix $\mathbf{C}^* = \mathbf{Q}^T \mathbf{C} \mathbf{Q}$.

$$\mathbf{C} = (\mathbf{Q}^T)^{-1} \mathbf{C}^* \mathbf{Q}^{-1}$$

$$= \mathbf{M} \mathbf{Q} (\mathbf{M}^*)^{-1} \mathbf{C}^* (\mathbf{M}^*)^{-1} \mathbf{Q}^T \mathbf{M} = \mathbf{M} \mathbf{Q} \hat{\mathbf{C}} \mathbf{Q}^T \mathbf{M}$$

$$\hat{\mathbf{C}} = \text{diag}(2\xi_i \omega_i).$$

If the eigenmode matrix has been mass orthogonalized, then $\mathbf{C} = \mathbf{M} \mathbf{\Phi} \hat{\mathbf{C}} \mathbf{\Phi}^T \mathbf{M}$.